Inorganic Chemistry

Article

pubs.acs.org/IC

A Family of Layered Chiral Porous Magnets Exhibiting Tunable Ordering Temperatures

Matteo Atzori,[†] Samia Benmansour,[‡] Guillermo Mínguez Espallargas,[‡] Miguel Clemente-León,[‡] Alexandre Abhervé,[‡] Patricia Gómez-Claramunt,[‡] Eugenio Coronado,[‡] Flavia Artizzu,[†] Elisa Sessini,[†] Paola Deplano,[†] Angela Serpe,[†] Maria Laura Mercuri,*[,†] and Carlos J. Gómez García*[,‡]

[†]Dipartimento di Scienze Chimiche e Geologiche, Università degli Studi di Cagliari, S.S. 554, Bivio per Sestu, I09042 Monserrato, Cagliari, Italy

[‡]Instituto de Ciencia Molecular (ICMol), Parque Científico, Universidad de Valencia, c/Catedrático José Beltrán, 2, 46980 Paterna, Valencia, Spain

Supporting Information

ABSTRACT: A simple change of the substituents in the bridging ligand allows tuning of the ordering temperatures, T_c, in the new family of layered chiral magnets $A[M^{II}M^{III}(X_2An)_3]\cdot G$ ($A = [(H_3O)(phz)_3]^+$ (phz = phenazine) or NBu_4^+; X_2An^{2-} = $C_6O_4X_2^{2-}$ = 2,5-dihydroxy-1,4-benzoquinone derivative dianion, with M^{III} = Cr, Fe; M^{II} = Mn, Fe, Co, etc.; X = Cl, Br, I, H; G = water or acetone). Depending on the nature of X, an increase in T_c from ca. 5.5 to 6.3, 8.2, and 11.0 K (for X = Cl, Br, I, and H, respectively) is observed in the MnCr derivative. Furthermore, the presence of the chiral cation $[(H_3O)(phz)_3]^+$, formed by the association of a hydronium ion with three phenazine molecules, leads to a chiral structure where the Δ-$[(H_3O)(phz)_3]^+$ cations are always located below the Δ-$[Cr(Cl_2An)_3]^{3-}$ centers, leading to a very unusual localization of both kinds of metals (Cr and Mn) and to an eclipsed disposition of the layers. This eclipsed disposition generates hexagonal channels with a void volume of ca. 20% where guest molecules (acetone and water) can be reversibly absorbed. Here we present the structural and magnetic characterization of this new family of anilato-based molecular magnets.

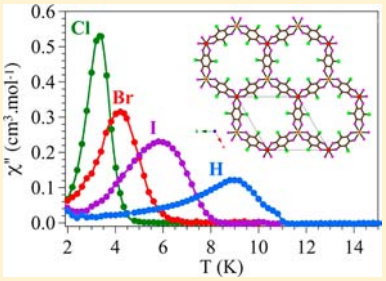

INTRODUCTION

The search for new molecule-based magnets is a very active area in molecular magnetism since these materials provide unique opportunities to design, from a wise selection of the molecular building blocks, crystal structures exhibiting cooperative magnetism and even the combination of magnetism with a second property of interest.[1−7] A breakthrough in this area was the preparation in 1992 by Okawa et al.[8] of the family of layered bimetallic oxalato-bridged magnets formulated as $[NBu_4][M^{II}Cr(C_2O_4)_3]$ (M^{II} = Mn, Fe, Co, Ni, Cu) with the well-known 2D hexagonal honeycomb structure[9,10] that orders ferromagnetically (M^{III} = Cr) with ordering temperatures (T_c) ranging from 6 to 14 K or ferrimagnetically (M^{III} = Fe) with T_c ranging from 19 to 48 K.[11−15]

In the last 20 years, many efforts have been addressed to include an additional property in these hybrid materials by playing with the functionality of the A^+ cations located between the bimetallic layers. This simple strategy has ed a large series of multifunctional molecular materials where the magnetic ordering of the bimetallic layer coexists and even interacts with other properties arising from the cationic layers such as paramagnetism,[12−16] nonlinear-optical properties,[17,18] metallic conductivity,[19,20] photochromism,[18,21,22] photoisomerism,[23] spin crossover,[24−29] chirality,[30−33] or proton conductivity.[34,35]

Still, the nature of the inserted cation affects very little (if any) the magnetic properties of the resulting hybrid material. Thus, the ordering temperatures (T_c) of these layered magnets are insensitive to the layer separation determined by the inserted cations, emphasizing their 2D magnetic character.[11−16,30,36,37]

Hence, the most effective way to tune the magnetic properties of these compounds is to act directly on the exchange pathways within the bimetallic layers. This can be done either by varying M^{II} and M^{III} or by modifying the bridging ligand ($C_2O_4^{2-}$). So far, only the first possibility has been explored (except for a few attempts at replacing the bridging oxalato ligand by the dithioxalato one, leading to a small variation in the ordering temperatures).[38−41]

To overcome this drawback, we have attempted the use of larger bis-bidentate bridging ligands as the dianion of 2,5-dihydroxy-1,4-benzoquinone (H_2dhbq) and its derivatives ($C_6O_4X_2^{2-}$ = X_2An^{2-}; Scheme 1) since they show coordination modes similar to the oxalato ligand and present three additional advantages: (i) they are easy to modify or functionalize in order to tune the exchange coupling through them by simply changing the X group (X = H, F, Cl, Br, I, NO_2, OH, CN, Me,

Received: May 27, 2013
Published: August 22, 2013

 © 2013 American Chemical Society

Scheme 1. $dhbq^{2-}$, X_2An^{2-}, and the Phenazine Molecules

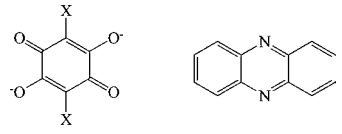

X = H ($dhbq^{2-}$)
X = Cl, Br or I (X_2An^{2-})

phenazine (phz)

Et, etc.);[42] (ii) their modification does not affect their coordination mode; (iii) they are able to provide an effective pathway for the exchange interaction.

The coordination modes and ability to act as bridging ligands of these anilato derivatives to afford many different coordination frameworks have been summarized by Kitagawa and Kawata.[42] Thus, the ligand $dhbq^{2-}$ and its derivatives, mainly with X = Cl (chloranilate), have been extensively studied, alone or in combination with other ligands (mainly nitrogen-donor ones), to prepare several compounds with different dimensionalities and structures, spanning from isolated monomers, dimers, and oligomers to extended 1D, 2D, and 3D structures.[42] One of the most interesting structures so far obtained are the honeycomb layers formed with $dhbq^{2-}$ and its chlorine derivative (chloranilate, Cl_2An^{2-}; Scheme 1).[43−48] In these 2D compounds, the structure is similar to that shown by the oxalato honeycomb layers, although all the reported examples to date are homometallic (i.e., they contain two M^{II} or two M^{III} ions instead of one M^{II} and one M^{III} ions). The layers formed with two M^{II} ions contain a 2− charge per formula, $[M^{II}_2L_3]^{2-}$ (L^{2-} = $dhbq^{2-}$ or X_2An^{2-}), and, accordingly, contain two monocations to balance the charge. To date, the only known examples of this $[M^{II}_2L_3]^{2-}$ series are $[M_2(dhbq)_3]^{2-}$ (M^{II} = Mn, Cd)[43] and $[M_2(Cl_2An)_3]^{2-}$ (M = Cu, Co, Cd, Zn).[44] With two M^{III} ions, the layers are neutral, and the reported examples to date include X = H, $[M^{III}_2(dhbq)_3]\cdot 24H_2O$ (M^{III} = Y, La, Ce, Gd, Yb, Lu),[45,46] X = Cl, $[M^{III}_2(Cl_2An)_3]\cdot 12H_2O$ (M^{III} = Sc, Y, La, Pr, Nd, Gd, Tb, Yb, Lu),[46,47] and X = Br, $[Y_2(Br_2An)_3]\cdot 12H_2O$.[47]

An additional interest of the $dhbq^{2-}$ and X_2An^{2-} ligands is related to the formation of a 3D structure with a (10,3)-a topology, similar to the one observed with oxalate,[49] which results when all of the ML_3 units present the same chirality (in contrast with the 2D honeycomb layer, which requires alternating Λ-ML_3 and Δ-ML_3 units). This 3D structure with a (10,3)-a topology has been recently reported for $[NBu_4]_2[M^{II}_2(dhbq)_3]$ (M^{II} = Mn, Fe, Ni, Co, Zn, Cd) and $[NBu_4]_2[Mn_2(Cl_2An)_3]$.[50] Albeit, in these compounds, the presence of a double-interpenetrating (10,3)-a lattice with opposite chiralities s a nonchiral structure. A final proof of the versatility of the anilate-derivative ligands is the formation of a 3D adamantane-like network in the compounds $Ag_2(Cl_2An)$,[51] $(H_3O)[Y(Cl_2An)_3]\cdot 8CH_3OH$, and $[Th(Cl_2An)_2]\cdot 6H_2O$.[46]

Unfortunately, the magnetic properties of the only two magnetically characterized 2D derivatives ($[M^{II}_2(Cl_2An)_3]^{2-}$, with M^{II} = Mn, Cu) lack interest because they show weak antiferromagnetic (AF) M−M interactions mediated by the Cl_2An^{2-} bridges (θ = −3.8 and −10.2 K for the copper and manganese derivatives, respectively).[44,48]

Since these ligands mediate AF exchange interactions, we can anticipate that the 2D heterometallic lattices of the type $[M^{II}M^{III}(X_2An)_3]^-$ should afford ferrimagnetic couplings and orderings. Furthermore, if, as expected, the magnetic coupling depends on the substituent groups X of the ligand, a change in X is expected to modify the magnetic coupling and T_c. This is probably the most interesting and appealing aspect of the anilato ligands since they can act as the oxalato ligands, but in contrast with this last one, they can be easily functionalized with different X groups. This possibility is expected to lead to an easy modulation of the electronic density in the ring, which should result in an easy tuning of the magnetic exchange coupling and, therefore, of the magnetic properties as the ordering temperatures and coercive fields in the resulting 2D or 3D magnets. It is to be noted that, to date, this has never been achieved because the ligands used to produce the series of molecular-based magnets (such as the oxalato, azido, or cyano ones) do not present any functionalization capacity as the anilato does. To check these appealing possibilities, we have synthesized and characterized the series of layered compounds $[(H_3O)(phz)_3][MnM^{III}(X_2An)_3]\cdot H_2O$ (phz = phenazine), with M^{III}/X = Cr/Cl (**1**), Cr/Br (**2**), and Fe/Br (**3**) and $[NBu_4][MnCr(X_2An)_3]$, with X = Cl (**4**), Br (**5**), I (**6**), and H (**7**). Here we report the X-ray crystal structure of compounds **1**−**4** and the magnetic characterization of all of the samples.

EXPERIMENTAL SECTION

General Remarks. Phenazine (phz = $C_{12}H_6N_2$), chloranilic acid (H_2Cl_2An), bromanilic acid (H_2Br_2An), 2,5-dihydroxy-1,4-benzoquinone (H_2dhbq), and the metal chloride salts are commercially available and were used as received without further purification. Iodanilic acid (H_2I_2An) was synthesized according to the literature methods.[52,53] $[Fe^{III}(sal_2\text{-epe})]ClO_4$ was synthesized as described in the literature,[54] where sal_2-epe is a Schiff base obtained by condensation of *N*,*N*′-bis(2-aminoethyl)-1,3-propanediamine and salicylaldehyde in a 1:2 ratio.

Synthesis of $[NBu_4]_3[Cr(Cl_2An)_3]$ (A). An aqueous solution (5 mL) of $CrCl_3\cdot 6H_2O$ (210 mg, 0.80 mmol) was added dropwise to an aqueous solution (50 mL) of H_2Cl_2An (500 mg, 2.4 mmol), NaOH (200 mg, 5.0 mmol), and NBu_4Br (800 mg, 2.5 mmol). After ca. 30 min at 60 °C, **A** precipitated as a red-brown solid, partially soluble in water. The mixture was allowed to cool to 25 °C, extracted with CH_2Cl_2, and dried under Na_2SO_4. The solution was filtered and rotoevaporated, and the obtained lacquer-like solid was crystallized in a $MeOH/CH_2Cl_2$ mixture to give red shiny crystals. Yield: 73%. Elem anal. Calcd for $C_{66}H_{108}Cl_6CrN_3O_{12}$: C, 56.61; H, 7.77; N, 3.00. Found: C, 56.38; H, 7.71; N, 2.83. FT-IR (ν_{max}/cm^{-1}, KBr pellets): 2962(m), 2933(w), 2875(m), 1649(m), 1531(vs), 1469(w), 1383(w), 1353(s), 1303(m), 1000(m), 880(w), 841(m), 739(vw), 612(m), 597(w), 572(w), 508(w), 447(w). UV−vis [CH_3CN solution; λ_{max}/nm (ε/$dm^3\cdot mol^{-1}\cdot cm^{-1}$)]: 466 sh, 497 (4493), 570 sh. UV−vis−NIR diffuse reflectance (λ_{max}/nm, KBr pellet): 200−675 (cutoff) broad, 800 sh.

Synthesis of $[NBu_4]_3[Cr(Br_2An)_3]$ (B). This compound was synthesized as red shiny crystals according to the procedure described above for **A**, using $CrCl_3\cdot 6H_2O$ (61 mg, 0.22 mmol), H_2Br_2An (194 mg, 0.65 mmol), NaOH (52 mg, 1.3 mmol), and NBu_4Br (213 mg, 0.66 mmol). Yield: 70%. Elem anal. Calcd for $C_{66}H_{108}Br_6CrN_3O_{12}$: C, 47.55; H, 6.53; N, 2.52. Found: C, 47.22; H, 6.43; N, 2.33. FT-IR (ν_{max}/cm^{-1}, KBr pellets): 2962(m), 2933(w), 2873(m), 1638(m), 1620(m), 1530(vs), 1343(s), 1310(m), 989(m), 883(w), 813(m), 736(w), 613(m), 594(w), 559(m), 507(m), 472(vw), 413(w). UV−vis [CH_3CN solution; λ_{max}/nm (ε/$dm^3\cdot mol^{-1}\cdot cm^{-1}$)]: 455 (4347), 490 (5115), 455 sh. UV−vis−NIR diffuse reflectance (λ_{max}/nm, KBr pellets): 200−714 (cutoff) broad, 817 sh.

Synthesis of $[NBu_4]_3[Cr(I_2An)_3]$ (C). This compound was synthesized as dark-red shiny crystals according to the procedure described above for **A**, using $CrCl_3\cdot 6H_2O$ (88 mg, 0.33 mmol), H_2I_2An (392 mg, 1.0 mmol), NaOH (80 mg, 2.0 mmol), and NBu_4Br (387 mg, 1.2 mmol). Yield: 74%. Elem anal. Calcd for $C_{66}H_{108}I_6CrN_3O_{12}$: C, 40.67; H, 5.59; N, 2.16. Found: C, 40.37; H, 5.32; N, 2.10. FT-IR

dx.doi.org/10.1021/ic4013284 | *Inorg. Chem.* 2013, 52, 10031−10040

(ν_{max}/cm^{-1}, KBr pellets): 2962(m), 2933(w), 2873(m), 1636(s), 1517(vs), 1334(s), 1295(w), 974(w), 919(vw), 878(w), 791(m), 738(w), 606(m), 548 (m), 504(m), 464(vw), 409(w). UV−vis (CH_3CN solution; λ_{max}/nm [ε/dm^3·mol^{-1}·cm^{-1})]: 463 sh, 502 sh, 627 sh. UV−vis−NIR diffuse reflectance (λ_{max}/nm, KBr pellets): 200−750 (cutoff) broad, 850 sh.

Synthesis of [NBu$_4$]$_3$[Fe(Br$_2$An)$_3$] (D). This compound was synthesized as dark-violet shiny crystals according to the procedure described above for **A**, using $FeCl_3$ (35 mg, 0.22 mmol), H_2Br_2An (194 mg, 0.65 mmol), NaOH (52 mg, 1.3 mmol), and NBu_4Br (213 mg, 0.66 mmol). Yield: 75%. Elem anal. Calcd for $C_{66}H_{108}Br_6FeN_3O_{12}$: C, 47.44; H, 6.52; N, 2.52. Found: C, 46.98; H, 6.31; N, 2.48. FT-IR (ν_{max}/cm^{-1}, KBr pellets): 2962(m), 2933(w), 2875(m), 1640(m), 1620(m), 1530(vs), 1472(m), 1338(s), 1281(m), 978(m), 883(w), 803(m), 739(w), 576(m), 564(m), 500(w). UV−vis [CH_3CN solution; λ_{max}/nm (ε/dm^3·mol^{-1}·cm^{-1})]: 443 (5487), 477 (6439), 519 (6841). UV−vis−NIR diffuse reflectance (λ_{max}/nm, KBr pellets): 200−950 (cutoff) broad.

Synthesis of [(H$_3$O)(phz)$_3$][MnCr(Cl$_2$An)$_3$(H$_2$O)] (1). Single crystals of this compound were obtained by carefully layering, at room temperature, a solution of **A** (14 mg, 0.01 mmol) in acetone (2 mL) on top of a solution of phenazine (54 mg, 0.3 mmol) in tetrahydrofuran (THF; 2 mL) and a solution of $MnCl_2·4H_2O$ (28 mg, 0.14 mmol) in water (2.5 mL). The solution was allowed to stand for about 3 months to obtain dark-purple/brown hexagonal prismatic crystals (together with a purple powder). Crystals suitable for X-ray diffraction were filtered and air-dried. Elem anal. Calcd for $C_{54}H_{29}N_6O_{14}Cl_6CrMn$: C, 49.68; H, 2.24; N, 6.44. Found: C, 49.31; H, 2.12; N, 6.30.

Synthesis of [(H$_3$O)(phz)$_3$][MnCr(Br$_2$An)$_3$]·H$_2$O·2CH$_3$COCH$_3$·H$_2$O (2). This compound was prepared like **1** but using **B** (16.7 mg, 0.01 mmol) instead of **A** and 108 mg (0.6 mmol) of phz. The crystallization time was ca. 1.5 months. Elem anal. Calcd for $C_{60}H_{41}N_6O_{16}Br_6CrMn$: C, 42.68; H, 2.45; N, 4.98. Found: C, 42.41; H, 2.40; N, 5.03.

Synthesis of [(H$_3$O)(phz)$_3$][MnFe(Br$_2$An)$_3$]·H$_2$O (3). This compound was prepared like **1** but using **D** (16.7, 0.01 mmol) instead of **A** and 108 mg (0.6 mmol) of phz. The crystallization time was ca. 1.5 months. Elem anal. Calcd for $C_{54}H_{29}N_6O_{14}Br_6FeMn$: C, 41.15; H, 1.86; N, 5.33. Found: C, 40.91; H, 1.80; N, 5.40.

Synthesis of [NBu$_4$][MnCr(Cl$_2$An)$_3$] (4). This compound was prepared by adding dropwise a solution of $MnCl_2·4H_2O$ (22 mg, 0.11 mmol) in MeOH (5 mL) to a solution of **A** (150 mg, 0.11 mmol) in CH_2Cl_2 (25 mL). Compound **4** precipitates immediately as a microcrystalline violet solid. The product was filtered, washed with CH_2Cl_2, and dried in an oven at 60 °C. Yield: 80%. Single crystals of this compound were prepared in a serendipitous way by carefully layering a solution of **A** (42 mg, 0.03 mmol) in acetonitrile (3 mL) on top of a solution of [Fe^{III}(sal)$_2$epe](ClO$_4$) (16 mg, 0.03 mmol) and $MnCl_2·4H_2O$ (6 mg, 0.03 mmol) in 3 mL of a 9:1 dichloromethane/methanol mixture. The solution was allowed to stand for about 3 weeks to obtain dark-purple prismatic single crystals. Elem anal. Calcd for $C_{34}H_{36}Cl_6MnCrNO_{12}$: C, 42.09; H, 3.74; N, 1.44. Found: C, 41.23; H, 4.43; N, 1.44. FT-IR (ν_{max}/cm^{-1}, KBr pellets): 2962(m), 2936(w), 2874(m), 1616(m), 1516(vs), 1360(s), 1310(w), 1006(s), 882(w), 856(s), 736(m), 624(m), 578(m), 511(m), 454(m). UV−vis−NIR diffuse reflectance (λ_{max}/nm, KBr pellets): 200−950 (cutoff) broad.

Synthesis of [NBu$_4$][MnCr(Br$_2$An)$_3$] (5). This compound was synthesized according to the procedure described above for **4**, using 16 mg (0.08 mmol) of $MnCl_2·4H_2O$ and 133 mg (0.08 mmol) of **B**. Attempts to prepare single crystals of this compound have been unsuccessful to date. Yield: 60%. Elem anal. Calcd for $C_{34}H_{36}Br_6MnCrNO_{12}$: C, 33.01; H, 2.93; N, 1.13. Found: C, 32.23; H, 2.78; N, 1.06. FT-IR (ν_{max}/cm^{-1}, KBr pellets): 2962(m), 2936(w), 2874(m), 1621(m), 1521(vs), 1487(vs), 1347(s), 990(w), 816(m), 610(m), 563(m), 507(m), 458(w), 407(w). UV−vis−NIR diffuse reflectance (λ_{max}/nm, KBr pellets): 200−960 (cutoff) broad.

Synthesis of [NBu$_4$][MnCr(I$_2$An)$_3$] (6). This compound was synthesized according to the procedure described above for **4**, using 16 mg (0.08 mmol) of $MnCl_2·6H_2O$ and 156 mg (0.08 mmol) of **C**. Attempts to prepare single crystals of this compound have been unsuccessful to date. Yield: 60%. Elem anal. Calcd for $C_{34}H_{36}I_6MnCrNO_{12}$: C, 26.88; H, 2.39; N, 0.92. Found. C, 26.12; H, 2.15; N, 0.75. FT-IR (ν_{max}/cm^{-1}, KBr pellets): 2959(m), 2931(w), 2871(w), 1621(m), 1495(vs), 1335(s), 974(m), 794(m), 609(m), 553(m), 506(m), 458(m). UV−vis−NIR diffuse reflectance (λ_{max}/nm, KBr pellets): 200−1050 (cutoff) broad.

Synthesis of [NBu$_4$][MnCr(dhbq)$_3$] (7). An aqueous solution (5 mL) of $CrCl_3·6H_2O$ (320 mg, 1.2 mmol) was added dropwise to a hot aqueous solution (50 mL) of H_2dhbq (500 mg, 3.6 mmol), NaOH (290 mg, 7.2 mmol), and NBu_4Br (1160 mg, 3.6 mmol). After ca. 30 min at T = 60 °C, a red-brown solid, partially soluble in water, precipitates. The mixture was allowed to cool to room temperature, extracted with CH_2Cl_2, and dried under Na_2SO_4. After filtration to remove Na_2SO_4, a solution of $MnCl_2·6H_2O$ (22 mg, 0.12 mmol) in MeOH (5 mL) was added dropwise to the CH_2Cl_2 solution. Compound **7** precipitates immediately as a microcrystalline violet solid. The product was filtered, washed with CH_2Cl_2, and dried in an oven at 60 °C. Attempts to prepare single crystals of this compound have been unsuccessful to date. Yield: 75%. Elem anal. Calcd for $C_{34}H_{42}MnCrNO_{12}$: C, 53.48; H, 5.54; N, 1.83. Found. C, 52.87; H, 5.32; N, 1.78. FT-IR (ν_{max}/cm^{-1}, KBr pellets): 2963(m), 2931(w), 2874(w), 1589(w), 1580(w), 1510(vs), 1424(m), 1396(s), 1365(s), 1251(s), 833(m), 823(m), 766(w), 720(w), 680(w), 587(m), 557(w), 543(w), 492(m), 442(w).

Structural Characterization. Single crystals of compounds **1**−**4** were mounted on glass fibers using a viscous hydrocarbon oil to coat the crystal and then transferred directly to the cold-nitrogen stream for data collection. X-ray data were collected at 130 K (**1**) or 120 K (**2**−**4**) on a Supernova diffractometer equipped with a graphite-monochromated Enhance (Mo) X-ray source (λ = 0.71073 Å). The program *CrysAlisPro*, Oxford Diffraction Ltd., was used for unit cell determinations and data reduction. Empirical absorption correction was performed using spherical harmonics, implemented in the SCALE3 ABSPACK scaling algorithm. **1** crystallizes in the trigonal chiral $P3$ space group, whereas **2** and **3** crystallize in the centrosymmetric $P\bar{3}1m$ space group and **4** in the centrosymmetric $C2/c$ space group. This difference might arise from the use of different haloanilato ligands (in **1**−**3**) and a different cation (in **4**). Crystal structures of **1**−**3** have been solved in both the $P3$ and $P\bar{3}1m$ space groups, but no suitable models have been found except as reported here. In addition, different data sets on different single crystals have been collected for each compound, and the results are consistent. Crystal structures were solved and refined against all F^2 values using the *SHELXTL* suite of programs.[55] Non-hydrogen atoms were refined anisotropically (when no disorder was present), and hydrogen atoms were assigned fixed isotropic displacement parameters. Hydrogen atoms of the phenazine ligand were placed in calculated positions that were refined using idealized geometries (riding model), and hydrogen atoms associated with oxygen atoms were located from the difference map with the O−H distance fixed at 0.86 Å.

In **1**, the chloranilate ligand, the Mn^{II} center, and the coordinated water molecule are disordered over two sites and have been modeled with a 49.8(8):50.2(2) ratio. In **2** and **3**, the increase of symmetry from $P3$ to $P\bar{3}1m$ provokes that the M^{III} and Mn^{II} centers cannot be differentiated and have been refined in the same position with a 50:50 ratio. In **2**, there is a disorder between the H_2O and H_3O^+ molecules, which have been refined with a common thermal parameter, whereas in **3**, H_2O and H_3O^+ lie in the same position and, thus, cannot be differentiated. The presence of solvent molecules in the structure voids has been analyzed with *PLATON/SQUEEZE*[56] when a suitable model has not been found (**1** and **3**). In **1**, no electron density is found in the voids, while in **3**, 12 electrons per void are found possibly because of the presence of a small amount of disordered acetone molecules. In **2**, the voids are filled with two acetone molecules, which have been modeled with a disorder of over six orientations each, with the carbon atoms of the C=O groups lying at the C3 axis. One thermal parameter has been used for each acetone molecule, and their hydrogen atoms were not modeled. A summary of the data collection and structure refinements is provided in Table 1.

dx.doi.org/10.1021/ic4013284 | Inorg. Chem. 2013, 52, 10031−10040

Table 1. Crystallographic Data for Compounds 1−4

	1	2	3	4
empirical formula	$C_{54}H_{29}N_6O_{14}Cl_6CrMn$	$C_{60}H_{41}N_6O_{16}Br_6CrMn$	$C_{54}H_{29}N_6O_{14}Br_6FeMn$	$C_{34}H_{36}NO_{12}Cl_6CrMn$
fw	1305.47	1688.39	1576.08	970.28
cryst color	red	black	black	brown
cryst size	0.05 × 0.05 × 0.04	0.10 × 0.07 × 0.05	0.11 × 0.03 × 0.03	0.09 × 0.06 × 0.03
temperature (K)	130(2)	120(2)	120(2)	120(2)
Wavelength (Å)	0.71073	0.71073	0.71073	0.71073
cryst syst, Z	trigonal, 1	trigonal, 1	trigonal, 1	monoclinic, 4
space group	$P3$	$P\bar{3}1m$	$P\bar{3}1m$	$C2/c$
a (Å)	13.7991(2)	13.7999(5)	13.9147(2)	13.776(5)
b (Å)	13.7991(2)	13.7999(5)	13.9147(2)	23.339(5)
c (Å)	9.0281(3)	9.2118(6)	9.1747(4)	16.833(5)
α (deg)	90	90	90	90
b (deg)	90	90	90	101.476(5)
γ (deg)	120	120	120	90
V (Å^3)	1488.77(6)	1519.24(13)	1538.40(7)	5304(3)
ρ_{calc} (Mg/m^3)	1.456	1.845	1.701	1.215
μ(Mo Kα) (mm^{-1})	0.731	4.407	4.402	0.791
θ range (deg)	3.41−25.05	1.70−25.00	2.93−27.50	3.02−25.13
reflns collected	28640	6252	23232	11965
indep reflns (R_{int})	3511 (0.0661)	975(0.0602)	1270 (0.0553)	4453 (0.132)
reflns used in refinement, n	3511	975	1270	4453
least-squares parameters, p/restraints, r	269/6	72/3	66/1	164/31
absolute structure parameter	0.06(4)	na	na	na
R1(F),[a] $I > 2\sigma(I$	0.0559	0.1352	0.0557	0.1584
wR2(F^2),[b] all data	0.1763	0.3272	0.2157	0.4721
$S(F^2)$,[c] all data	1.110	1.240	1.153	1.302

[a] $R1(F) = \sum||F_o| - |F_c||/\sum|F_o|$. [b] $wR2(F^2) = [\sum w(F_o^2 - F_c^2)^2/\sum wF_o^4]^{1/2}$. [c] $S(F^2) = [\sum w(F_o^2 - F_c^2)^2/n + r - p)]^{1/2}$.

In compound **4**, the small size of the crystals gave rise to very weak scattering and to a low number of reflections, precluding an anisotropic refinement of all the atoms, which was only applied to the heavy ones. Thus, carbon, nitrogen, and oxygen atoms could only be modeled isotropically. This caused high R1 and wR2 values. The tetrabutylammonium cation is disordered over two positions and required restraints and exclusion of the hydrogen atoms. This caused several A- and B-type alerts in the checkcif report. Nevertheless, although the disorder in the butyl chains of the cations precludes a very precise resolution of the structure, the presence of a layered structure, where the anionic layer is identical with that of **1**, is clearly established.

Physical Properties. Fourier transform infrared (FT-IR) spectra were performed on KBr pellets and collected with a Bruker Equinox 55 spectrophotometer. Electronic spectra (1200−200 nm) were recorded in a CH_3CN solution on a Varian Cary 5 spectrophotometer. Diffuse-reflectance spectra (2000−200 nm) were performed on KBr pellets and were acquired with a Varian Cary 5 spectrophotometer. Carbon, hydrogen, and nitrogen analyses were performed with a Thermo Electron CHNS Flash 2000 analyzer and with a Carlo Erba model EA1108 CHNS analyzer. Thermogravimetric analysis (TGA) was done on a polycrystalline sample (m = 6.24 mg) of compound **1** crystallized from an acetone/water/THF mixture using a Mettler-Toledo TGA/SDTA 851e analyzer with a sensibility of 10^{-7} g. The powder X-ray diffractometer was collected for a polycrystalline sample of **4** filled into a 0.3 mm glass capillary that was mounted and aligned on a Empyrean PANalytical powder diffractometer, using Cu Kα radiation (λ = 1.54177 Å). A total of two scans were collected at room temperature in the 2θ range of 2−60°.

Magnetic Properties. Magnetic measurements were performed with a Quantum Design MPMS-XL-5 SQUID magnetometer in the 2−300 K temperature range with an applied magnetic field of 0.1 T on polycrystalline samples of all the compounds with masses of 0.23, 1.77, 3.18, and 0.79 mg for the single-crystalline phases **1**−**4**, respectively, and 14.21, 4.23, 16.00, and 15.07 mg for the powder samples **4**−**7**, respectively. Note that sample **4** was measured as single crystals and as a microcrystalline powder to confirm that both samples present the same magnetic properties. The hysteresis measurements were done with fields from −5 to +5 T at different temperatures below T_c after cooling the samples in zero field. Alternating-current (ac) susceptibility measurements were performed on the same samples with an oscillating magnetic field of 0.395 mT at low temperatures in the frequency range 1−1000 Hz. Susceptibility data were corrected for the sample holder and for the diamagnetic contribution of the salts using Pascal's constants.[57]

RESULTS AND DISCUSSION

Synthesis. The anilate-based molecular magnets have been obtained by following the so-called "complex-as-ligand approach". In this synthetic strategy, a molecular building block, the homoleptic $[M^{III}(X_2An)_3]^{3-}$ tris-anilate metalate octahedral complex (M^{III} = Cr, Fe),[58] is used as a ligand toward divalent metal cations (M^{II} = Mn, Fe, Co, etc.). Their combination results in the formation of 2D anionic complexes, which precipitate in the presence of a bulky organic cation, i.e., $[NBu_4]^+$. In these compounds, monovalent cations act not only as charge-compensating counterions but also as templating agents that control the dimensionality of the final system. Moreover, the choice of the interacting metal ions and the bridging ligand plays a key role in tuning the nature and magnitude of the magnetic interaction between the metal ions, especially when the bridge contains weak electronegative groups that may act as "adjusting screws".[59]

The growth of single crystals of the heterometallic 2D layers was not a simple task since all attempts to obtain single crystals from a mixture of the $[NBu_4]^+$ salts of the $[M^{III}(X_2An)_3]^{3-}$ precursors with the M^{II} chlorides yielded very poorly crystalline or amorphous materials. The crystallization process required the addition of phenazine, which, in the presence of hydronium

dx.doi.org/10.1021/ic4013284 | Inorg. Chem. 2013, 52, 10031−10040

cations $(H_3O)^+$, forms the chiral cation $[(H_3O)(phz)_3]^+$, which seems to template the crystallization process. Interestingly, while trying to include other cations between the layers, such as the spin-crossover complex $[Fe^{III}(sal)_2epe]^+$, we have unexpectedly obtained single crystals of the $[NBu_4]^+$ salt **4**. This result suggests that the solvent or the presence of the Fe^{III} complex may play an important role in facilitating inclusion of the $[NBu_4]^+$ cations. Attempts are in progress to study the role of these and other factors (such as the concentration, cation of the precursor $[M^{III}(X_2An)_3]^{3-}$ salt, etc.) in the formation of single crystals for different $[M^{III}M^{II}(X_2An)_3]^-$ derivatives.

IR Spectroscopy. The mononuclear precursor **A** shows in the central region of the IR spectrum two bands, centered at ca. 1000 and 841 cm^{-1}, which can be assigned according to the literature to the ν(C−C), ν(C−O), δ(C−Cl) and δ(C═O), δ(C−O), ν(C−Cl) combination bands.[60] These peaks are typical of the chloranilato ligand and are affected by its coordination to the metals because they involve the vibrational modes of the chelating group. Thus, the FT-IR spectrum of the heterometallic layered compound **4** shows a clear shift to higher wavenumbers of these two bands (which now appear at ca. 1007 and 857 cm^{-1}; Figure S1 in the Supporting Information, SI) upon coordination of the Cl_2An^{2-} ligand to the Mn^{II} centers, suggesting a stronger structural rigidity of the anilato ring when acting as a bridging ligand, as was already observed in the related heterometallic oxalate-based layers.[8] The IR spectra of compounds **5** and **6** show a similar shift toward lower wavenumbers upon coordination of the corresponding anilate derivative to the Mn^{II} center. Furthermore, as expected, the IR spectra of compounds **4**−**6** show a shift of these bands toward lower wavenumbers as the mass of X increases (Figure S2 in the SI). These facts suggest that the X_2An^{2-} ligands (X = Cl, Br, I) exhibit the same coordination mode and support the idea that compounds **4**−**6** are isostructural, in agreement with the magnetic measurements (see below).

Powder X-ray Diffraction. The isostructurality of the two samples prepared of compound **4** was confirmed with the experimental and simulated powder X-ray diffractograms, which were very similar (Figure S3 in the SI). Unfortunately, compounds **5**−**7** could only be prepared as very poorly polycrystalline samples, and their composition and structure can only be inferred from elemental analysis, a detailed study of the IR spectra, and their magnetic properties.

TGA. TGA of a polycrystalline sample of **1** shows a total weight loss of ca. 8.7% in the temperature range 25−130 °C with a plateau above ca. 125 °C (Figure S4 in the SI). This weight loss corresponds to the release of two acetone molecules and half a water molecule per formula unit (calcd value = 8.7%), in good agreement with the X-ray data of **2**. Note that although the crystal used for the structure determination of **1** did not show any electron density in the hexagonal channels, the corresponding polycrystalline sample contains solvent molecules, as demonstrated by TGA analysis. This difference can be due to the different synthetic methods used to prepare the single crystals (3 months of layering) and the polycrystalline sample (immediate precipitation in a one-pot reaction).

Single-Crystal X-ray Structures. Compounds **1**−**3** are isostructural and present a layered structure with alternating cationic and anionic layers (Figure 1). The only differences between compounds **1**−**3**, besides the change of Cl_2An^{2-} by Br_2An^{2-} (**1** vs **2**) or chromium by iron (**2** vs **3**), are (i) the presence of an inversion center in compounds **2** and **3** (but not in **1**), resulting in a statistical distribution of the M^{III} and Mn^{II} ions in the anionic layers (see the Experimental Section) and (ii) the presence of a water molecule coordinated to the Mn^{II} ions in **1** [Mn−O1w = 2.379(17) Å], in contrast with compounds **2** and **3**, where this water molecule is not coordinated [Mn−O1w = 3.123(3) and 4.587(6) Å in **2** and **3**, respectively]. The presence of the water molecule is probably due to two factors: (i) the change in the X group (chlorine in **1** vs bromine in **2** and **3**) and (ii) the presence of an inversion center in **2** and **3** (absent in **1**). Thus, in **1**, the two chlorine atoms are expected to produce an important electron-withdrawing effect on the anilate ring and, indirectly, on the oxygen atoms, leading to weaker (and, therefore, longer) Mn−O bonds [Mn1−O5 = 2.182(8) Å and Mn1−O6 = 2.273(9) Å]. This elongation of the six Mn−O bonds allows the approach and coordination of an additional water molecule. In compounds **2** and **3**, the bromine atoms are less electron-withdrawing, leading to stronger (and, therefore, shorter) M−O bonds [M−O2 = 2.102(13) and 2.119(4) Å in **2** and **3**, respectively, i.e., ca. 8% and 7% shorter than that in **1**]. This shortening of the M−O bonds is also due to the fact that the metallic positions in **2** and **3** are a statistical average of (smaller) M^{III} ions and Mn^{II} ones. Both effects point to a more difficult approach of the water molecule to the Mn^{II} atom in **2** and **3**, as observed in their structures. Furthermore, this approach is more hindered in **3** than in **2**, in agreement with the longer Mn···OH_2 distance in **3**.

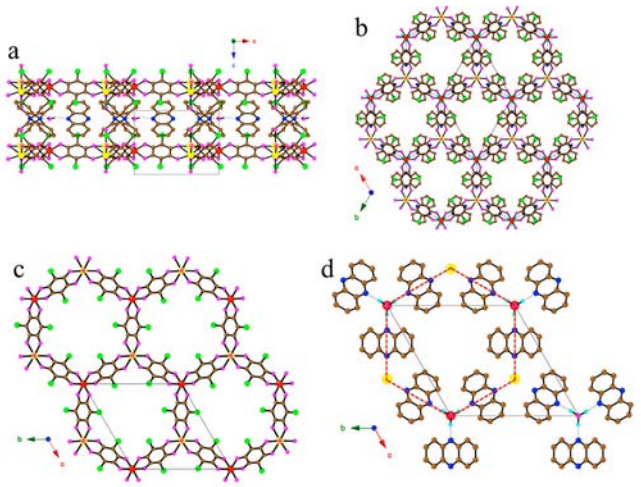

Figure 1. Structure of compound **1**: (a) Side view of the alternating cationic and anionic layers. (b) Top view of the two layers. (c) Top view of the anionic layer. (d) Top view of the cationic layer showing the positions of the metal centers in the anionic layer (red dashed hexagon). Color code: C = brown, O = pink, *N* = blue, H = cyan, Cl = green, Mn = yellow, Cr = red.

Since compounds **1**−**3** present essentially the same structure (except for the slight differences already indicated), we will focus on the structure of compound **1**. The structure is formed by cationic and anionic layers parallel to the *ab* plane alternating along the *c* direction (Figure 1). The anionic layer can be formulated as $[Mn^{II}Cr^{III}(Cl_2An)_3(H_2O)]^-$ ($[Mn^{II}Cr^{III}(Br_2An)_3]^-$ in **2** and $[Mn^{II}Fe^{III}(Br_2An)_3]^-$ in **3**) and presents the classical hexagonal honeycomb layer where the Cr^{III} and Mn^{II} ions, connected through the anilate bis-bidentate ligands, occupy alternating vertices of the hexagons (Figure 1). Each Mn^{II} ion is connected to three Cr^{III} ions and vice versa (Figure 2).

dx.doi.org/10.1021/ic4013284 | *Inorg. Chem.* 2013, 52, 10031−10040

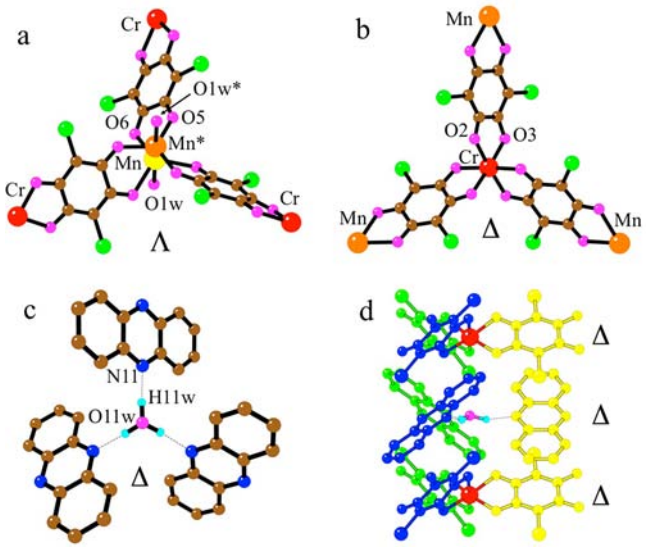

Figure 2. Structural building units of compound **1**: (a) Λ-$[Mn(Cl_2An)_3(H_2O)]^{4-}$ entity connected to three Cr^{III} ions showing the two equally possible locations of the H_2O molecule and the Mn^{II} ion (orange and yellow); (b) Δ-$[Cr(Cl_2An)_3]^{3-}$ entity connected to three Mn^{II} ions; (c) Δ-$[(H_3O)(phz)_3]^+$ cation showing the O–H···N bonds as dotted lines; (d) side view of two anionic and one cationic layers showing Δ-$[(H_3O)(phz)_3]^+$ and the Δ-$[Cr(Cl_2An)_3]^{3-}$ entities located above and below. Parallel phenazine and anilato rings are displayed with the same color. Color code in a–c: C, brown; O, pink; N, blue; H, cyan; Cl, green; Mn, yellow/orange; Cr, red.

Although this structure is similar to that of the homometallic $[M_2(X_2An)_3]^{n-}$ derivatives (n = 0 or 2),[43−48] there are three important differences: (i) Compounds **1**–**3** are heterometallic and monoanionic (i.e., contain two different metal ions with two different oxidation states, M^{III} and Mn^{II}, resulting in a charge of 1− per formula unit or per hexagon in the layer since each hexagon contains one formula unit $[M^{II}M^{III}(X_2An)_3]^-$). (ii) In **1**, the metal ions are perfectly ordered (in contrast to **2** and **3** and almost all the heterometallic oxalato layers) due to the absence of an inversion center in the center of the hexagon as a result of the chirality of this structure. (iii) In **1**, the Mn^{II} ions (but not the Cr^{III} ones) present a coordinated water molecule perpendicular to the layers, either above or below (Figure 2), producing a displacement of the Mn^{II} ions of 0.59 Å with respect to the average plane defined by the Cr^{III} ions. Since the water molecules are statistically distributed over the two possible locations, the Mn^{II} ions are also disordered on two close positions with a Mn–Mn distance of 1.18 Å (the Mn–O1w bond is perpendicular to the layer; Figure 2). The presence of a water molecule coordinated to the Mn^{II} ion in **1** implies the counterintuitive conclusion that the H_3O^+ cation is located closer to the Cr^{III} ion than to the Mn^{II} ion. The extra difference in the repulsion energies between the H_3O^+–Cr^{III} and H_3O^+–Mn^{II} dispositions has to be overcome by the extra Mn–OH_2 bond. This idea agrees with the assumption that all the Mn^{II} ions are coordinated to a water molecule and, therefore, that the disorder affects both the Mn^{II} and water positions simultaneously. Note that the opposite distribution where the Cr^{III} ion would be heptacoordinated and the Mn^{II} ion hexacoordinated has to be excluded given the smaller size of Cr^{III} compared to Mn^{II} and the fact that the metal ions present typical Mn^{II}–O and Cr^{III}–O distances. In fact, any attempt to change the metal ions led to significantly worse structural refinements.

The cationic layer is formed by chiral entities formulated as Δ-$[(H_3O)(phz)_3]^+$ (Figure 2c) resulting from the association of three phenazine molecules around a central H_3O^+ cation through three equivalent strong O–H···N hydrogen bonds [O–H = 0.97(2) Å, H···N = 1.73(3) Å, O···N = 2.663(4) Å, and O–N···H = 160(7)°], generating a propeller-like structure. These Δ-$[(H_3O)(phz)_3]^+$ entities are always located below and above the Δ-$[Cr(Cl_2An)_3]^{3-}$ units since they present the same chirality, allowing a parallel orientation of the phz and Cl_2An^{2-} rings (Figure 2d). This fact suggests a chiral recognition during the synthetic process between oppositely charged [Cr-$(Cl_2An)_3]^{3-}$ and $[(H_3O)(phz)_3]^+$ precursors with the same configuration (Δ or Λ). Note that this disposition leads to an unexpected situation where the more highly charged cation Cr^{III} is located closer to the hydronium cation while the less charged cation Mn^{II} is located closer to the water molecule. As indicated above, this extra repulsion is overcome by the Mn–OH_2 bond energy.

An additional interest of compounds **1**–**3** is that they present hexagonal channels resulting from the eclipsed packing of the cationic and anionic layers (Figure 3). These channels may

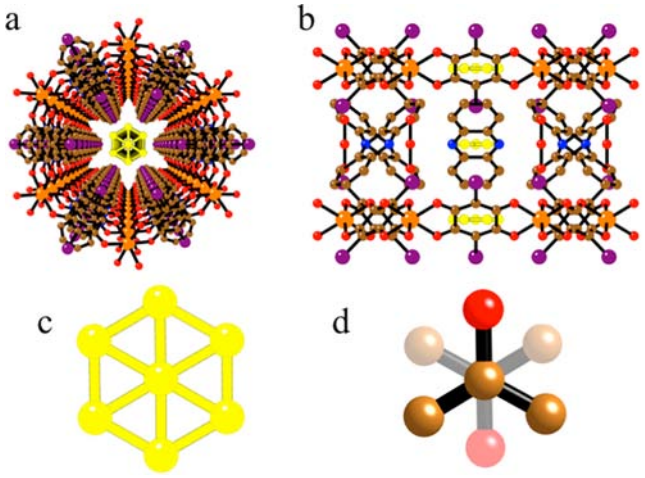

Figure 3. Structure of $[(H_3O)(phz)_3][MnCr(Br_2An)_3]\cdot H_2O\cdot 2CH_3COCH_3\cdot{}^1/_2H_2O$ (**2**): (a) perspective view of one hexagonal channel running along the c direction with the solvent molecules in the center (in yellow); (b) side view of the same hexagonal channel showing the location of the solvent molecules in the center of the anionic and cationic layers; (c) disordered solvent molecules as observed in the center of the hexagonal channels; (d) view of two possible orientations of the CH_3COCH_3 molecules in the channels. Color code in parts a, b, and d: C, brown; O, red; N, blue; Br, violet; Mn/Cr, orange.

contain solvent molecules. Thus, in **2** (and to a lesser extent in **3**), X-ray crystal structure analysis shows the presence in the channels of electron density distributed in a centered planar hexagon (Figure 3c) located in the center of both layers (Figure 3b). This density can be attributed to the presence of two acetone molecules per formula unit with two different orientations related by a 2-fold axis (Figure 3c,d). Once assigned the electron density corresponding to the two acetone molecules, there is a small residual density that may be assigned to $^1/_2$ water molecule, in agreement with TGA (see above). Interestingly, in some homometallic $[M_2(Cl_2An)_3]^{2-}$ lattices, two acetone and two water molecules were also observed.[44]

dx.doi.org/10.1021/ic4013284 | Inorg. Chem. 2013, 52, 10031−10040

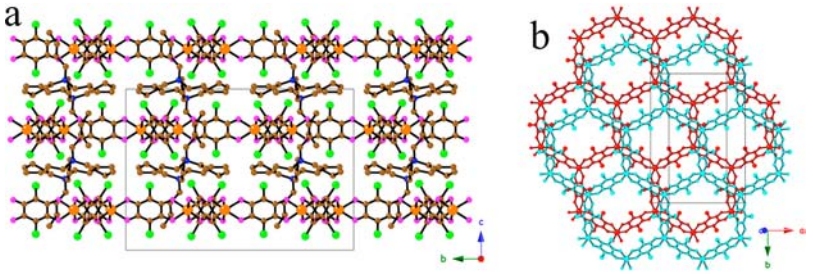

Figure 4. Structure of **4**: (a) view of the alternating anionic and cationic layers; (b) projection, perpendicular to the layers, of two consecutive anionic layers showing their alternate packing.

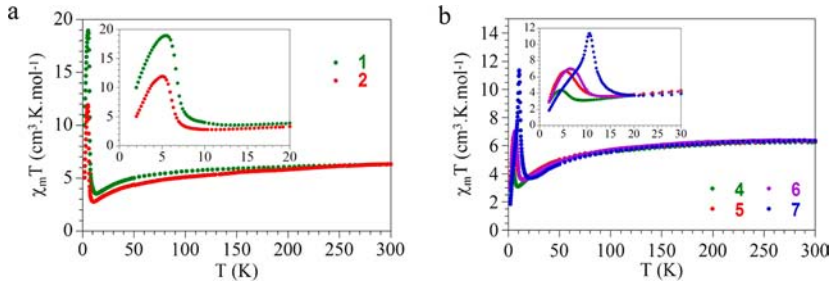

Figure 5. Magnetic properties of compounds **1**, **2**, and **4**–**7**: (a) thermal variation of $\chi_m T$ for **1** and **2**; (b) thermal variation of $\chi_m T$ for **4**–**7**. Insets show the low-temperature regions.

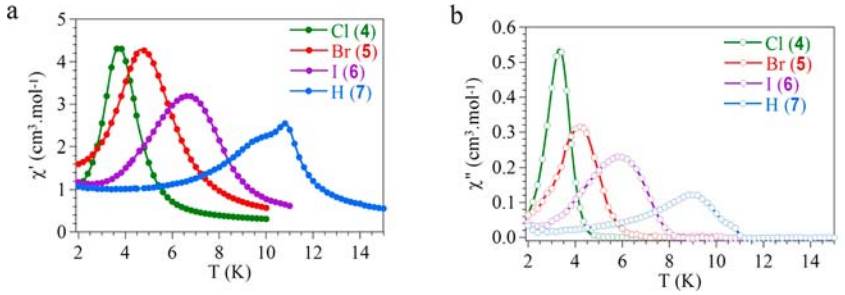

Figure 6. Magnetic properties of the series of $[NBu_4][MnCr(X_2An)_3]$, X = Cl (**4**), Br (**5**), I (**6**) and H (**7**): (**a**) Thermal variation of the in phase (χ_m') AC susceptibility at 1 Hz. (**b**) Thermal variation of the out of phase (χ_m'') AC susceptibility at 1 Hz.

The only compound with the $[NBu_4]^+$ cation whose structure has been solved, **4**, shows a similar layered structure with hexagonal anionic $[MnCr(Cl_2An)_3]_n^{n-}$ layers alternating with cationic layers containing disordered $[NBu_4]^+$ cations. The main differences between **4** and **1**–**3** are the lack of a water molecule coordinated/located close to the Mn^{II} ion and, more importantly, the absence of hexagonal channels since in **4** the honeycomb layers are not eclipsed but alternated (Figure 4).

Magnetic Properties. The magnetic measurements of the two crystalline compounds with the $[H_3O(phz)_3]^+$ cation and chromium and manganese in the anionic layer, **1** and **2**, show the presence of AF chromium–manganese interactions mediated through the X_2An^{2-} bridges, as is clearly shown by the thermal variation of their magnetic moment (represented as the product of the molar magnetic susceptibility per $Mn^{II}Cr^{III}$ couple times the temperature, $\chi_m T$). Since the ground spin states of Cr^{III} and Mn^{II} are different ($^3/_2$ and $^5/_2$, respectively) this AF interaction leads to a ferrimagnetic coupling that results in a ferrimagnetic long-range ordering at low temperatures. Thus, $\chi_m T$ shows at room temperature values of 6.20 and 6.24 $cm^3 \cdot K \cdot mol^{-1}$, for **1** and **2**, respectively, close to the expected one (6.25 $cm^3 \cdot K \cdot mol^{-1}$ for $g = 2$) for a noninteracting couple of Mn^{II} and Cr^{III} ions. When the temperature is lowered, $\chi_m T$ shows a continuous decrease (since the magnetic coupling is AF and the total magnetic moment is reduced as the temperature decreases), reaching a minimum at ca. 10 K (since the two ground spin states are not fully canceled), followed by a sharp increase at lower temperatures and a maximum at ca. 5 K, indicating the presence of a long-range ferrimagnetic ordering (Figure 5a).

This behavior is similar to that of the $[NBu_4]^+$ salts containing the $[MnCr(X_2An)_3]^-$ layers [X = Cl (**4**), Br (**5**), I (**6**), H (**7**); Figure 5b]. Thus, compounds **4**–**7** show $\chi_m T$ values at room temperature of ca. 6.2 $cm^3 \cdot K \cdot mol^{-1}$ that decrease when the temperature is lowered to reach minima at ca. 9.3, 13.5, 14.3, and 21.5 K, followed by sudden increases with maximum slopes at ca. 5.7, 7.0, 8.6, and 11.2 K and maxima at ca. 4.5, 5.5, 6.5, and 10.5 K for X = Cl, Br, I, and H, respectively (inset in Figure 5b). This behavior confirms the presence of ferrimagnetic Mn^{II}–Cr^{III} interactions with long-range ferrimagnetic orderings at ca. 5.7, 7.0, 8.6, and 11.2 K for **4**–**7**, respectively.

This shift of the ordering temperature as the X group varies from Cl to Br, I, and H suggests that T_c increases as the electronegativity of X decreases, as will be discussed later.

dx.doi.org/10.1021/ic4013284 | Inorg. Chem. 2013, 52, 10031–10040

To confirm the long-range order and obtain a more accurate value for T_c, we have performed susceptibility measurements with an oscillating magnetic field at different frequencies in the range 1−1000 Hz (ac susceptibility). These measurements show frequency-independent peaks in both the in-phase (χ_m') and out-of-phase (χ_m'') susceptibilities in all compounds, confirming the presence of long-range ordering (Figure 6). Furthermore, compounds **1** and **4** present similar magnetic properties, confirming that both compounds contain the same magnetic $[MnCr(Cl_2An)_3]^-$ lattices. On the other hand, compounds **2** and **5** also show the same properties, confirming the assumption that both contain the same magnetic lattice ($[MnCr(Br_2An)_3]^-$ in this case). Albeit, the peaks observed in the crystalline samples (**1** and **2**) are narrower than those observed for the $[NBu_4]^+$ salts (**4** and **5**) (Figure S5 in the SI), suggesting the presence of a larger structural and occupational disorder and a larger number of vacancies in the metal-ion positions in the less crystalline samples (**4** and **5**).

Although all the samples show similar ac behaviors, the positions of the peaks change with X, as is also observed in the DC magnetic measurements. Thus, for compounds **4**−**7**, respectively, the peaks in the in-phase susceptibility, χ_m', appear at ca. 3.7, 4.7, 6.6, and 10.8 K (Figure 6a), and in the out-of-phase (χ'') susceptibility, they appear at ca. 3.3, 4.2, 5.9, and 9.1 K (Figure 6b). T_c, determined as the temperature at which χ'' becomes nonzero, is ca. 5.5, 6.3, 8.2, and 11.0 K for **4**−**7**, respectively.

The ferrimagnetic nature of the coupling in all the manganese−chromium compounds is further confirmed by the isothermal magnetization measurements at 2 K that show a smooth increase of the magnetization with increasing fields and no saturation even at high fields (Figure 7). These measurements also provide an additional proof of the magnetic ordering presented by these layered materials because all compounds present hysteresis below the ordering temperatures with coercive fields of ca. 11.8, 27.0, 4.5, and 92.0 mT for **4**−**7**, respectively (Figure 7). The hysteresis measurements at 2 K performed on the single-crystalline samples (compounds **1** and **2**; Figure S6 in the SI) show coercive fields (19.4 and 34.0 mT for **1** and **2**, respectively) that are slightly higher than those of the corresponding polycrystalline $[NBu_4]^+$ salts (11.8 and 27.0 mT for **4** and **5**, respectively). A similar effect was observed in the oxalate-based layers and was attributed to the different packings of the anionic layers (eclipsed vs alternated).[14]

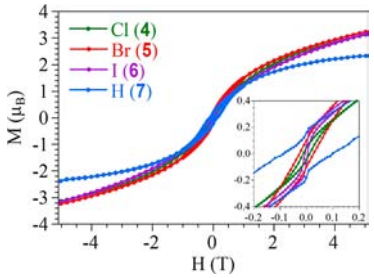

Figure 7. Hysteresis cycles at 2 K for the series $[NBu_4][MnCr(X_2An)_3]$, where X = Cl (**4**), Br (**5**), I (**6**), and H (**7**). The inset shows the low-field region of the hysteresis cycles.

The only Fe^{III} derivative (**3**) shows a $\chi_m T$ value at room temperature of ca. 8.8 $cm^3 \cdot K \cdot mol^{-1}$ (close to the one expected, 8.75 $cm^3 \cdot K \cdot mol^{-1}$, for a couple of noninteracting Fe^{III} and Mn^{II} ions with $g = 2$) and an AF coupling, as evidenced by a continuous decrease of $\chi_m T$ as the temperature is lowered to 2 K (Figure 8). A close inspection at the low-temperature data of the χ_m vs T plot (inset in Figure 8) shows a sharp maximum at ca. 4 K, suggesting the presence of a long-range AF ordering. In compound **3**, the ac measurements show a weak peak in the in-phase (χ_m') and out-of-phase (χ_m'') susceptibilities at ca. 3.5 K, suggesting the presence of a long-range AF ordering with spin canting (weak ferromagnetism; Figure S7 in the SI). This situation, already observed in the related MnFe derivatives of the oxalate-based bimetallic series,[11,61] is due to the presence of a canting angle between the spin of both ions that prevents a perfect antiparallel alignment of the corresponding spins. This canting leads to an incomplete cancellation of the magnetic moments, resulting in a weak ferromagnetic ordering of the noncanceled components.

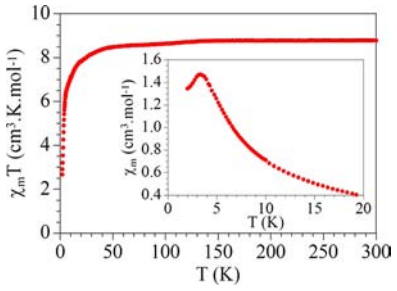

Figure 8. Thermal variation of $\chi_m T$ for compound **3**. The inset shows the low-temperature region for χ_m.

In the chromium−manganese compound, the presence of long-range ferrimagnetic orderings may be anticipated from the expected AF chromium−manganese interaction through the X_2An^{2-} bridges.[42,44,48] The heterometallic nature of the 2D lattice with two different spin ground states (except in the iron−manganese derivative) leads to the observed ferrimagnetic long-range ordering.

As was already stated, a very interesting result observed in the chromium−manganese series is the change in T_c as X changes in this family of layered ferrimagnets. Furthermore, the order observed in T_c (Cl < Br < I < H) suggests that the electronegativity of X may play a key role in determining T_c. Actually, a plot of T_c versus the electronegativity of X shows a clear linear correlation (Figure 9) that can be easily explained with the electron-withdrawing effect of X: as the electronegativity of X increases, the electron density in the anilato ring

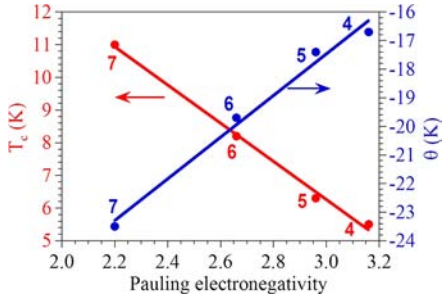

Figure 9. Linear dependence of the ordering temperature (T_c, left scale, red) and the Weiss temperature (θ, right scale, blue) with the electronegativity of the X group in the series $[NBu_4][MnCr(X_2An)_3]$, where X = Cl (**4**), Br (**5**), I (**6**), and H (**7**). Solid lines are the corresponding linear fits.

dx.doi.org/10.1021/ic4013284 | Inorg. Chem. 2013, 52, 10031−10040

decreases, resulting in a weaker coupling and, therefore, in a lower T_c. Indeed, the fit of the molar susceptibility of compounds **4**–**7** to the Curie–Weiss law [$\chi_m = C/(T - \theta)$; Figure S8 in the SI] shows a linear increase in the absolute value of the Weiss temperature (θ, corresponding to the magnitude to the magnetic coupling) as the electronegativity of X decreases. Thus, the strength of the ferrimagnetic coupling increases with a decrease in the electronegativity of X, with θ = −16.7(2), −17.4(1), −19.7(2), and −23.5(2) K for **4**–**7**, respectively (Figure 9). This fact demonstrates that it is possible (and easy) to tune T_c in these series by simply changing the X group in the anilato derivative.

CONCLUSIONS

Compounds **1**–**4** are the first structurally (and magnetically) characterized heterometallic honeycomb anilate-bridged bimetallic layers and demonstrate the versatility of using anilato derivatives as bridging ligands to obtain bimetallic 2D ferrimagnets. A second interesting aspect of the anilato derivatives is the possibility that they offer to tune the ordering temperatures by simply changing the substituents in the anilato bridging ligand. Thus, compounds **4**–**7** show that T_c values vary linearly with the electronegativity of the X group. As is also observed in the oxalato derivatives, we have also shown that it is possible to tune the magnetic properties by changing the M^{III} and M^{II} ions as observed in compounds **2** and **3**. Furthermore, preliminary measurements in some poorly crystalline $[NBu_4]^+$ salts of different $[M^{II}M^{III}(X_2An)_3]^-$ anions show ordering temperatures between ca. 3 and 6 K for the Fe^{II}–Cr^{III} and Co^{II}–Cr^{III} derivatives.

A third interesting feature of this family is that compound **1** is chiral because it contains the chiral cation $[(H_3O)(phz)_3]^+$, yielding a very unusual ordered arrangement of the metals in the layer and an eclipsed disposition of the layers. This eclipsed disposition generates a fourth interesting feature in these compounds: the presence of hexagonal channels that can be filled with different guest molecules. Thus, compounds **1**–**3** present a void volume of ca. 291 Å^3 (ca. 20% of the unit cell volume), where solvent molecules can be absorbed, opening the way to the synthesis of new porous magnets. Compound **1** is, therefore, the first structurally (and magnetically) characterized porous chiral layered magnet based on anilato-bridged bimetallic layers. This chirality is expected to be of interest for studying the magnetochiral effect as well as the multiferroic properties, as has already been done in the oxalato family.[32,49,62,63]

Furthermore, the bigger size of the anilato compared to the oxalato ligand leads to hexagonal cavities that are twice larger than those of the oxalato-based layers. This bigger size represents a fifth interesting feature of the anilato-based layers since it will allow the inclusion of a larger library of cations in order to prepare multifunctional molecular materials combining the magnetic ordering of the anionic layers with any additional property of the cationic one (the chirality of the $[(H_3O)(phz)_3]^+$ cation is only the first example). The synthesis of such derivatives including new cations bearing interesting functionalities is underway. In fact, a preliminary study reveals that it is possible to include different spin-crossover complexes between these magnetic layers.

Moreover, as was already done in the oxalato family,[49] the use of preformed chiral cations of the $[M(L)_3]^{n+}$ type (L = neutral bidentate ligand) is expected to a vast family of bimetallic chiral 3D magnets.

An extra possibility of the present series is that of including an additional functionality in the anilato-based bridge that, besides a tuning of the critical temperature (as shown here), may add an extra property and/or modify the properties (such as the hydrophobicity or nucleophilicity) as well as the size of the hexagonal channels since the X groups are directed toward the center of these channels. The use of anilato derivative ligands with other functional groups[42] such as NO_2, F, CN, OH, Me, Et, etc., is also underway.

ASSOCIATED CONTENT

Supporting Information

X-ray crystallographic data in CIF format, FT-IR spectra, powder X-ray diffractograms, TGA, detailed dc and ac magnetic properties, hysteresis curves, and Curie–Weiss plots. This material is available free of charge via the Internet at http://pubs.acs.org. CCDC 953846–953849 (**1**–**4**) contain the supplementary crystallographic data for this paper. These data can also be obtained free of charge from The Cambridge Crystallographic Data Centre via www.ccdc.cam.ac.uk/data_request/cif.

AUTHOR INFORMATION

Corresponding Author

*E-mail: mercuri@unica.it (M.L.M.), carlos.gomez@uv.es (C.J.G.G.). Phone: +39 070 6754486 (M.L.M.), +34 96 3544423 (C.J.G.G.). Fax: +39 070 6754456 (M.L.M.), +34 96 3543273 (C.J.G.G.).

Author Contributions

All authors have given approval to the final version of the manuscript.

Notes

The authors declare no competing financial interest.

ACKNOWLEDGMENTS

We thank the EU (SPINMOL ERC Adv. Grant), the Spanish MINECO (Projects Consolider-Ingenio in Molecular Nanoscience CSD2007-00010, CTQ-2011-26507, and MAT2011-22785), the Regione Autonoma della Sardegna, L.R. 7-8-2007, Bando 2009, CRP-17453 Project "Nano Materiali Multifunzionali per Applicazioni nell'Elettronica Molecolare", and the Generalitat Valenciana (Prometeo and ISIC-Nano programs) for financial support.

REFERENCES

(1) Miller, J. S.; Gatteschi, D. *Chem. Soc. Rev.* **2011**, *40*, 3065–3066.
(2) Sorace, L.; Benelli, C.; Gatteschi, D. *Chem. Soc. Rev.* **2011**, *40*, 3092–3104.
(3) Sugawara, T.; Komatsu, H.; Suzuki, K. *Chem. Soc. Rev.* **2011**, *40*, 3105–3118.
(4) Coronado, E.; Minguez Espallargas, G. *Chem. Soc. Rev.* **2013**, *42*, 1525–1539.
(5) Coronado, E.; Giménez-Marqués, M.; Mínguez Espallargas, G.; Brammer, L. *Nat. Commun.* **2012**, *3*, 828.
(6) Mercuri, M. L.; Deplano, P.; Serpe, A.; Artizzu, F. In *Multifunctional Nanomaterials of interest in Electronics*; Ouahab, L., Ed.; Pan Stanford Publishing: Singapore, 2013.
(7) Pilia, L.; Sessini, E.; Artizzu, F.; Yamashita, M.; Serpe, A.; Kubo, K.; Ito, H.; Tanaka, H.; Kuroda, S.; Yamada, J.; Deplano, P.; Gómez-García, C. J.; Mercuri, M. L. *Inorg. Chem.* **2012**, *52*, 423–430.
(8) Tamaki, H.; Zhong, Z. J.; Matsumoto, N.; Kida, S.; Koikawa, M.; Achiwa, N.; Hashimoto, Y.; Okawa, H. *J. Am. Chem. Soc.* **1992**, *114*, 6974–6979.

(9) Atovmyan, L. O.; Shilov, G. V.; Lyubovskaya, R. N.; Zhilyaeva, E. I.; Ovanesyan, N. S.; Pirumova, S. I.; Gusakovskaya, I. G.; Morozov, Y. G. *JETP Lett.* **1993**, *58*, 766−769.
(10) Decurtins, S.; Schmalle, H. W.; Oswald, H. R.; Linden, A.; Ensling, J.; Gütlich, P.; Hauser, A. *Inorg. Chim. Acta* **1994**, *216*, 65−73.
(11) Mathoniere, C.; Nuttall, C. J.; Carling, S. G.; Day, P. *Inorg. Chem.* **1996**, *35*, 1201−1206.
(12) Clemente-Leon, M.; Coronado, E.; Galan-Mascaros, J. R.; Gómez-García, C. J. *Chem. Commun.* **1997**, 1727−1728.
(13) Coronado, E.; Clemente-Leon, M.; Galan-Mascaros, J. R.; Gimenez-Saiz, C.; Gómez-García, C. J.; Martínez-Ferrero, E. *J. Chem. Soc., Dalton Trans.* **2000**, 3955−3961.
(14) Coronado, E.; Galan-Mascaros, J. R.; Gómez-García, C. J.; Ensling, J.; Gutlich, P. *Eur. J. Inorg. Chem.* **2000**, *6*, 552−563.
(15) Coronado, E.; Galan-Mascaros, J. R.; Gómez-García, C. J.; Martinez-Agudo, J. M. *Adv. Mater.* **1999**, *11*, 558−561.
(16) Coronado, E.; Galan-Mascaros, J. R.; Gómez-García, C. J.; Martinez-Agudo, J. M.; Martinez-Ferrero, E.; Waerenborgh, J. C.; Almeida, M. *J. Solid State Chem.* **2001**, *159*, 391−402.
(17) Benard, S.; Riviere, E.; Yu, P.; Nakatani, K.; Delouis, J. F. *Chem. Mater.* **2001**, *13*, 159−162.
(18) Bénard, S.; Yu, P.; Audière, J. P.; Rivière, E.; Clément, R.; Guilhem, J.; Tchertanov, L.; Nakatani, K. *J. Am. Chem. Soc.* **2000**, *122*, 9444−9454.
(19) Coronado, E.; Galan-Mascaros, J. R.; Gómez-García, C. J.; Laukhin, V. *Nature* **2000**, *408*, 447−449.
(20) Alberola, A.; Coronado, E.; Galan-Mascaros, J. R.; Gimenez-Saiz, C.; Gómez-García, C. J. *J. Am. Chem. Soc.* **2003**, *125*, 10774−10775.
(21) Aldoshin, S. M.; Nikonova, L. A.; Shilov, G. V.; Bikanina, E. A.; Artemova, N. K.; Smirnov, V. A. *J. Mol. Struct.* **2006**, *794*, 103−109.
(22) Aldoshin, S. M.; Sanina, N. A.; Minkin, V. I.; Voloshin, N. A.; Ikorskii, V. N.; Oveharenko, V. I.; Smirnov, V. A.; Nagaeva, N. K. *J. Mol. Struct.* **2007**, *826*, 69−74.
(23) Kida, N.; Hikita, M.; Kashima, I.; Okubo, M.; Itoi, M.; Enomoto, M.; Kato, K.; Takata, M.; Kojima, N. *J. Am. Chem. Soc.* **2008**, *131*, 212−220.
(24) Clemente-Leon, M.; Coronado, E.; Giménez-Lopez, M. C.; Soriano-Portillo, A.; Waerenborgh, J. C.; Delgado, F. S.; Ruiz-Perez, C. *Inorg. Chem.* **2008**, *47*, 9111−9120.
(25) Sieber, R.; Decurtins, S.; Stoeckli-Evans, H.; Wilson, C.; Yufit, D.; Howard, J. A. K.; Capelli, S. C.; Hauser, A. *Chem.—Eur. J.* **2000**, *6*, 361−368.
(26) Clemente-Leon, M.; Coronado, E.; Lopez-Jorda, M.; Minguez Espallargas, G.; Soriano-Portillo, A.; Waerenborgh, J. C. *Chem.—Eur. J.* **2010**, *16*, 2207−2219.
(27) Clemente-Leon, M.; Coronado, E.; Lopez-Jorda, M. *Dalton Trans.* **2010**, *39*, 4903−4910.
(28) Clemente-Leon, M.; Coronado, E.; Lopez-Jorda, M.; Waerenborgh, J. C. *Inorg. Chem.* **2011**, *50*, 9122−9130.
(29) Clemente-Leon, M.; Coronado, E.; Lopez-Jorda, M.; Desplanches, C.; Asthana, S.; Wang, H.; Letard, J. *Chem. Sci.* **2011**, *2*, 1121−1127.
(30) Gruselle, M.; Train, C.; Boubekeur, K.; Gredin, P.; Ovanesyan, N. *Coord. Chem. Rev.* **2006**, *250*, 2491−2500.
(31) Brissard, M.; Gruselle, M.; Malezieux, B.; Thouvenot, R.; Guyard-Duhayon, C.; Convert, O. *Eur. J. Inorg. Chem.* **2001**, 1745−1751.
(32) Train, C.; Gheorghe, R.; Krstic, V.; Chamoreau, L.; Ovanesyan, N. S.; Rikken, G. L. J. A.; Gruselle, M.; Verdaguer, M. *Nat. Mater.* **2008**, *7*, 729−734.
(33) Clemente-Leon, M.; Coronado, E.; Dias, J. C.; Soriano-Portillo, A.; Willett, R. D. *Inorg. Chem.* **2008**, *47*, 6458−6463.
(34) Sadakiyo, M.; Okawa, H.; Shigematsu, A.; Ohba, M.; Yamada, T.; Kitagawa, H. *J. Am. Chem. Soc.* **2012**, *134*, 5472−5475.
(35) Okawa, H.; Shigematsu, A.; Sadakiyo, M.; Miyagawa, T.; Yoneda, K.; Ohba, M.; Kitagawa, H. *J. Am. Chem. Soc.* **2009**, *131*, 13516−13522.
(36) Clement, R.; Decurtins, S.; Gruselle, M.; Train, C. *Monatsh. Chem.* **2003**, *134*, 117−135.
(37) Fishman, R. S.; Clemente-Leon, M.; Coronado, E. *Inorg. Chem.* **2009**, *48*, 3039−3046.
(38) Carling, S. G.; Bradley, J. M.; Visser, D.; Day, P. *Polyhedron* **2003**, *22*, 2317−2324.
(39) Bradley, J. M.; Carling, S. G.; Visser, D.; Day, P.; Hautot, D.; Long, G. J. *Inorg. Chem.* **2003**, *42*, 986−996.
(40) Kojima, N.; Aoki, W.; Itoi, M.; Ono, Y.; Seto, M.; Kobayashi, Y.; Maeda, Y. *Solid State Commun.* **2001**, *120*, 165−170.
(41) Okawa, H.; Mitsumi, M.; Ohba, M.; Kodera, M.; Matsumoto, N. *Bull. Chem. Soc. Jpn.* **1994**, *67*, 2139−2144.
(42) Kitagawa, S.; Kawata, S. *Coord. Chem. Rev.* **2002**, *224*, 11−34.
(43) Weiss, A.; Riegler, E.; Robl, C. *Z. Naturforsch., B: J. Chem. Sci.* **1986**, *41*, 1501−1505.
(44) Luo, T.; Liu, Y.; Tsai, H.; Su, C.; Ueng, C.; Lu, K. *Eur. J. Inorg. Chem.* **2004**, 4253−4258.
(45) Abrahams, B. F.; Coleiro, J.; Hoskins, B. F.; Robson, R. *Chem. Commun.* **1996**, 603−604.
(46) Abrahams, B. F.; Coleiro, J.; Ha, K.; Hoskins, B. F.; Orchard, S. D.; Robson, R. *J. Chem. Soc., Dalton Trans.* **2002**, 1586−1594.
(47) Christian, R. *Mater. Res. Bull.* **1987**, *22*, 1483−1491.
(48) Shilov, G. V.; Nikitina, Z. K.; Ovanesyan, N. S.; Aldoshin, S. M.; Makhaev, V. D. *Russ. Chem. Bull.* **2011**, *60*, 1209−1219.
(49) Coronado, E.; Galán-Mascarós, J. R.; Gómez-García, C. J.; Martínez-Agudo, J. M. *Inorg. Chem.* **2001**, *40*, 113−120.
(50) Abrahams, B. F.; Hudson, T. A.; McCormick, L. J.; Robson, R. *Cryst. Growth Des.* **2011**, *11*, 2717−2720.
(51) Frenzer, W.; Wartchow, R.; Bode, H. *Z. Kristallogr.* **1997**, *212*, 237−237.
(52) Torrey, H. A.; Hunter, W. H. *J. Am. Chem. Soc.* **1912**, *34*, 702−716.
(53) Stenhouse, J. *J. Chem. Soc.* **1870**, *23*, 6−14.
(54) Griffin, M.; Shakespeare, S.; Shepherd, H. J.; Harding, C. J.; Létard, J.; Desplanches, C.; Goeta, A. E.; Howard, J. A. K.; Powell, A. K.; Mereacre, V.; Garcia, Y.; Naik, A. D.; Müller-Bunz, H.; Morgan, G. G. *Angew. Chem., Int. Ed.* **2011**, *50*, 896−900.
(55) Sheldrick, G. M. *Acta Crystallogr., Sect. A* **2008**, *64*, 112−122.
(56) Spek, A. *J. Appl. Crystallogr.* **2003**, *36*, 7−13.
(57) Bain, G. A.; Berry, J. F. *J. Chem. Educ.* **2008**, *85*, 532−536.
(58) Atzori, M.; Artizzu, F.; Sessini, E.; Marchiò, L.; Serpe, A.; Deplano, P.; Benmansour, S.; Gómez-García, C. J.; Pop, F.; Avarvari, N.; Mercuri, M. L. Manuscript in preparation.
(59) Tinti, F.; Verdaguer, M.; Kahn, O.; Savariault, J.-M. *Inorg. Chem.* **1987**, *26*, 2380−2384.
(60) Pawlukojc, A.; Bator, G.; Sobczyk, L.; Grech, E.; Nowicka-Scheibe, J. *J. Phys. Org. Chem.* **2003**, *16*, 709−714.
(61) Carling, S. G.; Mathoniere, C.; Day, P.; Malik, K. M. A.; Coles, S. J.; Hursthouse, M. B. *J. Chem. Soc., Dalton Trans.* **1996**, 1839−1843.
(62) Cañadillas-Delgado, L.; Fabelo, O.; Rodríguez-Velamazán, J. A.; Lemée-Cailleau, M.; Mason, S. A.; Pardo, E.; Lloret, F.; Zhao, J.; Bu, X.; Simonet, V.; Colin, C. V.; Rodríguez-Carvajal, J. *J. Am. Chem. Soc.* **2012**, *134*, 19772−19781.
(63) Kherfi, H.; Hamadène, M.; Guehria-Laïdoudi, A.; Dahaoui, S.; Lecomte, C. *Materials* **2010**, *3*, 1281−1301.